Catalysis Science & Technology

Accepted Manuscript

ROYAL SOCIETY OF CHEMISTRY

www.rsc.org/catalysis

Catalysis Science & Technology

ARTICLE

The Role of Potassium Promoter for Isobutanol Synthesis on Zn-Cr Based Catalysts

Received 00th January 20xx,
Accepted 00th January 20xx

DOI: 10.1039/x0xx00000x

www.rsc.org/

Shaopeng Tian,[a, b] Sichen Wang,[c] Yingquan Wu, [a] Junwen Gao, [c] Peng Wang, [a, b] Hongjuan Xie, [a] Guohui Yang, [a] Yizhuo Han [a] and Yisheng Tan *[a]

A series of Zn-Cr oxide nanoparticles with different content of potassium promoter is obtained by a coprecipitation and postcalcined method. Transmission Electron Microscope (TEM), Powder X-Ray Diffraction (XRD), X-ray photoelectron spectroscopy (XPS) and Fourier Transform Infrared spectroscopy (FT-IR) were used to confirm the structure of different Zn-Cr oxides. The results demonstrate that the potassium promoter would tailor the microstructure of Zn-Cr spinel by affecting the cation distribution between tetrahedral and octahedral vacancies. Furthermore, the potassium promoter also affects tremendously oxygen state on the surface over Zn-Cr spinel. Both of the population and stability of oxygen species could be enhanced by potassium promoter. In addition, the surface hydroxyl species could facilitate the formate formation which is a very significant intermediate C1 species for alcohol synthesis. The catalyst activity and isobutanol selectivity are closely related to the content of potassium promoter, clearly demonstrating that potassium promoter should be one of crucial issues to enhance the catalytic performance for isobutanol formation over Zn-Cr catalysts.

1. Introduction

Increasing consumption of petroleum, demand for additives to increase the octane rating of gasoline, and concern about the environment will cause requirements for petroleum-free sources of value-added chemicals to increase in the future. [1-9] Isobutanol is one of the most important of the clean synthetic fuels and chemical intermediates that are produced from coal. [1, 2] Isobutanol has been found to be an effective and clean fuel, with a high octane rating, for automobiles. Isobutanol can also be used to produce a range of chemicals, including anti-aging chemicals, pharmaceuticals and plasticizers. The US Environmental Protection Agency approved the use of isobutanol as a gasoline additive in 2010. The rapid increase in the consumption of isobutanol that has occurred means that a low-cost method of manufacturing isobutanol is required. The non-noble-metal catalyst family based on $ZnCr_2O_4$ modified with potassium offers particular promise for achieving this aim. These catalysts have been studied widely because they remain very active for longer than many other catalysts, cause relatively little coke to be deposited, can cause higher alcohols to form, and are highly selective for the formation of isobutanol. [10-13]

Oxides based on Zn and Cr have been studied extensively since the 1980s, and thorough reviews of the work that has been performed on these oxides have been published. [14, 15] Members of our research group have performed a number of studies of the pathways and active sites involved in the formation of isobutanol from synthesis gas using Zn–Cr oxides. [1, 6, 16-18] We found that isobutanol is formed through the addition of a C_1 (formyl) intermediate to the α-carbon of methanol to give alcohols with two or more carbon atoms and then the aldol condensation of these alcohols. We also discovered that the level of cation disorder distribution in Zn-Cr spinel structure affects tremendously isobutanol formation. The role of potassium in the catalyst in promoting the reactions was not considered in any depth in our previous studies.

Alkali metal promoters are widely used in catalytic reactions of synthesis gas to improve the activities, selectivities, and stabilities of the catalysts. [19, 20] Doping a Zn–Cr catalyst with a small amount of an alkali metal can increase the amounts of higher alcohols (particularly isobutanol) formed. However, there is still some debate about the role of potassium in promoting the synthesis of higher alcohols using different catalysts. All authors of relevant studies have agreed that the presence of an alkali metal increases the chemical activity of a catalyst even though different authors started from different hypotheses that otherwise led to different conclusions. Lee et al. [20] concluded that, under the reaction conditions they used, a K_2CO_3 promoter readily removed counter-anions and caused a new complex (which they concluded was a carboxylic species) to form. The authors proposed that these carboxylic species were the active intermediates in the synthesis of alcohols from synthesis gas. Iranmahboob et al. [21] suggested that potassium causes the hydrogenation of different species on the catalyst to be slowed, by poisoning the hydrogenation sites, and increases the number of active sites available for the formation of higher alcohols. Sachtler et al. [22] suggested that the presence of an alkali metal affects the kinetics and energetics of the adsorption of hydrogen, carbon monoxide,

[a] State Key Laboratory of Coal Conversion, Institute of Coal Chemistry, Chinese Academy of Sciences, Taiyuan, Shanxi, China.
[b] University of the Chinese Academy of Sciences, Beijing, China.
[c] Shaanxi Yanchang Petroleum (Group) Corp. Ltd., Xi ′ an, P. R. China.
Electronic Supplementary Information (ESI) available: Temperature Programmed Desorption of CO (CO-TPD). See DOI:10.1039/x0xx00000x

and other reactants to the catalyst, thereby affecting the relative surface areas covered by these species during a reaction. Zaman et al. [23] suggested that an alkali metal can block sites on a MoS_2 surface, simultaneously increasing the non-dissociative adsorption of CO and decreasing the amount of hydrogen activation that occurs on the MoS_2 surface. Koizumi et al. [24] compared the catalytic properties of MoS_2 doped with different amounts of K, Cs, and Rb and with high and low surface areas. The optimum amounts of alkali promoters and the optimum species of alkali promoters were found to be very different for MoS_2 with a high surface area and for MoS_2 with a low surface area. Similar results were found by Liu et al. [25] These results clearly showed that the degree of promotion that occurs when MoS_2 is used as a catalyst depends on the surface area of the MoS_2. Some authors [23] have also suggested that adding potassium stabilizes oxygenated species, causing alcohols rather than hydrocarbons to be synthesized.

The studies described above very effectively improved our understanding of surface science and allowed the optimum amounts and species of alkali promoters that should be used to synthesize alcohols from synthesis gas to be determined. The effects of electron donation from the alkali metal to the metals that modify the states of the active sites and the ways that CO and H_2 bind to the surfaces of catalysts have also been studied many times. The dramatic changes that occur in the catalytic activities and selectivities of catalysts when very low loadings of alkali metal promoters are present can reasonably be explained from the results of these studies. Several remarkable studies of the synthesis of higher alcohols using MoS_2 catalysts with alkali metal promoters and using other catalysts have been reported, [23, 26] but Zn–Cr spinel catalysts (which are very important catalysts for synthesizing higher alcohols) have been studied relatively little. [27] Only co-adsorbed molecules on the surfaces of Zn–Cr catalysts have been studied previously, [11, 12] and the more interesting effects of alkali metals on the surface structures of Zn–Cr spinel catalysts have merely been taken into account.

In the study described here, we prepared Zn–Cr spinels containing different amounts of potassium and studied the role of the alkali metal in promoting the formation of isobutanol. In contrast with previous studies, we focused on determining how the alkali metal affected the surface structures of the Zn–Cr catalysts and why the presence of potassium on Zn–Cr spinel surfaces is strongly associated with the formation of isobutanol.

2. Experimental section

2.1 Preparation of catalysts

Zn-Cr oxides samples were prepared by a typical coprecipitation procedure. Appropriate amounts (the Zn/Cr molar ratio is 0.8) of starting materials $Zn(NO_3)_2{\cdot}6H_2O$ mixed $Cr(NO_3)_3{\cdot}9H_2O$ and $(NH_4)_2CO_3{\cdot}CH_3NO_2$ were dissolved in 800mL of deionized water, respectively. Then the two kinds of solutions were pumped together by peristaltic pumps in a well-stirred thermostated container with pH of 9 at 60 ^oC. Next, the dark green suspension was aged for 15h, then filtered, washed thoroughly by deionized water at 60 ^oC, and dried at 100 ^oC overnight. Dried samples was milled into powders and calcined at 350 ^oC for 6h to remove carbonates, etc. Then, the dark powders were impregnated with 0-6wt% K_2O as a promotor using potassium carbonate and the incipient wetness method. Finally, the catalysts were dried at 100 ^oC for 12h and calcined at 400 ^oC for 6h in order to form the corresponding Zn-Cr spinel or spinel-like oxides. Catalysts could be labeled as 0K-ZnCr, 1K-ZnCr, 3K-ZnCr and 6K-ZnCr, respectively. For the 3K-ZnCr, the '3K' represented the fraction of K_2O on the total catalyst weight is 3%, and the rest of catalysts are similar.

2.2 Characterization of catalysts

The morphology and microstructure of samples were investigated using a field emission transmission electron microscope (HRTEM, JEM-2100F) operated at 200kV. The XPS patterns were recorded using an AXIS ULTRA DLD X-ray photoelectron spectrometer, equipped with a multichannel detector. Charge referencing was done against adventitious carbon (C 1s, 284.8 eV). A Shirley-type background was subtracted from the signals. The recorded spectra were fitted using Gauss–Lorentz curves to determine the surface composition of different samples. FT-IR Spectra were obtained with a TENSOR-27 in the range from 4000 to 400 cm^{-1} with 4 cm^{-1} resolution. Before CO adsorption, all of catalysts were reduced with a 10% hydrogen-in-nitrogen mixture for 0.5 h at 400 ^oC online. CO adsorption was taken at 400 ^oC. After 0.5 h of pure Ar flow at the same temperature, the adsorbates existing on the surface of different Zn–Cr spinel catalysts would be measured. The procedure of CO-IR analysis was OPUS-65.

The X-ray diffraction (XRD) data of the samples were recorded using a D8 Advance X-ray diffractometer in a 2θ range from 25^o to 78^o with Cu Kα radiation. To obtain high quality XRD patterns for Rietveld analysis, scans were taken with a 2θ step size of 0.01^o and counting time of 2s for each point. All peak positions were used in the determination of precise microstrucural parameters. Crystalline Structural refinements were carried out with the Rietveld method by using the program of FP_Suite_TB, which is especially designed to refine simultaneously both the structural and microstructural parameters. The lattice parameters were deduced from XRD line positions using a least-squares refinement model. Peak shape profiles were fitted with a pseudo-Voight function and asymmetry parameters were considered for peaks below 45^o (2θ). The background was refined with a sixth coefficients function. Refinement continues till convergence is reached with the value of quality factor. The fit of the calculated pattern to the observed data can be given numerically: the weighted-profile value, R_{wp}, is defined as

$$R_{wp} = \left\{ \sum_i w_i \left[y_i(\text{obs}) - y_i(\text{calc}) \right]^2 \Big/ \sum_i w_i \left[y_i(\text{obs}) \right]^2 \right\}^{1/2}$$

Where $y_i(\text{obs})$ is the observed intensity at step i, $y_i(\text{calc})$ the calculated intensity, and w_i the weight. The expression in the numerator is the value that is minimized during a Rietveld refinement. In our computational process, R_{wp} ranged from 13.2% to 14.7% which confirmed the goodness of refinement.

Nitrogen adsorption–desorption isotherms were carried out at -195.8 ^oC using a Micromeritics ASAP 2020 analyzer. Before

adsorption, the samples were out-gassed at 350 °C for 10h. The specific surface area (S_{BET}) was evaluated using the BET method, while the pore size distribution was calculated according to the Barrett–Joyner–Halenda (BJH) formula applied to the desorption branch. The Temperature Programmed Reduction of hydrogen (H_2-TPR) was recorded on TP-5050 automatic chemical adsorption instrument in the range from 50 °C to 600 °C. For the sake of accuracy, pure standard mixtures [zeolite + activated carbon] were used during preliminary TPR measurements. 0.1g catalyst was used to test the redox properties of different catalysts. Firstly, the temperature was increased to 300 °C at a constant rate of 10 °C min^{-1} and pure Ar flowed for 60 min at that temperature to eliminate the adsorption of physically adsorbed water and impurities. Then, after the temperature was decreased to 50 °C, the temperature was increased to 600 °C at a constant rate of 5 °C min^{-1} under an appropriate amount of Ar flow. The desorbed species were analysed by thermal conductivity measurements.

2.3 Activity measurements.

Each of these catalysts was reduced with a 10% hydrogen-in-nitrogen mixture for 4 h at 400 °C on line. Then, these catalysts were tested for isobutanol catalytic activity in a fixed bed using a feed gas of 2.6:1 H_2 and CO mixture at a space velocity of 3,000 h^{-1}. The reactions were run at temperature 400 °C and pressure 10 MPa. The products were analyzed by four on-line GC during the reaction. Inorganic gas products consisted of CO, H_2, H_2O and CO_2 were detected online by thermal conductivity measurements using a GC4000A (carbon molecular sieves column). The organic gas products consisted of hydrocarbons and methanol were detected online by flame ionization measurements using a GC4000A (GDX-403 column). The alcohol products in liquid phase were detected by flame ionization measurements using a GC-7AG (Chromsorb101). The H_2O and methanol products in liquid phase were detected by thermal conductivity measurements using a GC4000A (GDX-401column).

3. Results and discussion

3.1. Morphology and microstructure of catalysts

Representative transmission electron microscopy (TEM) images of Zn–Cr nanocrystals with different potassium contents are shown in Fig. 1. The catalysts with different potassium contents all had particles of around 6 nm in diameter. The microstructures of the catalysts, determined by high resolution TEM, are shown in the insets of the subfigures in Fig. 1. The interplanar spacings (indicated by arrows) were found to be between 5.01 Å and 5.03 Å, which are very close to the ideal spacing (5.02 Å) for $ZnCr_2O_4$ facets (3 1 1). [28] The periodical lattice fringes indicated that each nanoparticle could be considered to be a good single crystal.

3.2. Texture parameters of catalysts

The texture parameters for the Zn–Cr samples are shown in Table 1. The Brunauer–Emmett–Teller surface areas (S_{BET}) of the Zn–Cr samples decreased linearly from 106 m^2 g^{-1} to 85.5 m^2 g^{-1} as the potassium content increased from 0% (by weight) to 6%. The pore volume (V_P) decreased linearly from 0.535 cm^3 g^{-1} to 0.235 cm^3 g^{-1} as the potassium content increased from 0% to 6%. The pore radius (R_P) decreased linearly from 17.4 nm to 8.59 nm as the potassium content increased from 0% to 6%.

Tab. 1. Texture parameters of catalysts

Catalysts	S_{BET}(m^2g^{-1})	V_p(cm^3g^{-1})	R_p(nm)
0K-ZnCr	106	0.535	17.4
1K-ZnCr	102	0.393	14.1
3K-ZnCr	95.4	0.304	11.7
6K-ZnCr	85.5	0.235	8.59

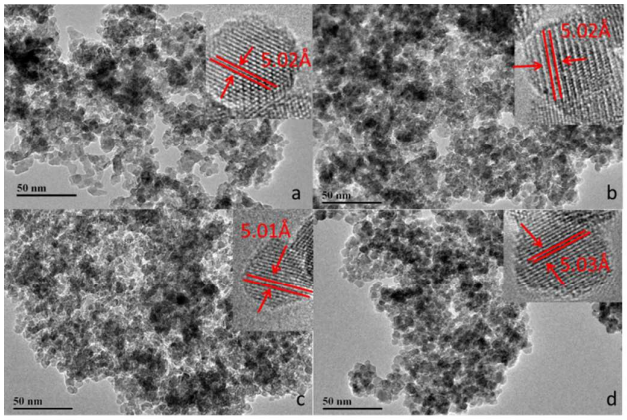

Fig. 1. TEM images of the catalysts with different contents of potassium, (a) 0K-ZnCr, (b) 1K-ZnCr, (c) 3K-ZnCr and (d) 6K-ZnCr.

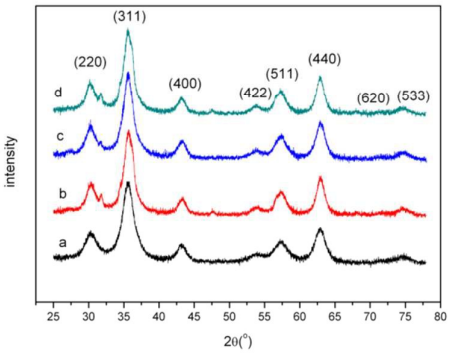

Fig.2. Powder XRD patterns of catalysts with different contents of potassium, (a) 0K-ZnCr, (b) 1K-ZnCr, (c) 3K-ZnCr and (d) 6K-ZnCr.

The measurements shown in Table 1 indicate that the texture parameters of the catalysts were slightly affected by the potassium content when the potassium content was less than 6%. The S_{BET}, V_P, and R_P would all have decreased as the potassium content increased because the potassium would have been unevenly distributed over the catalyst surfaces. An excess of unevenly distributed potassium will generally partly cover the sites responsible for the formation of isobutanol and negatively affect the catalyst performance. It was therefore necessary to determine the optimum potassium loading for the synthesis of isobutanol.

3.3 Characterization of the catalysts using powder X-ray diffractometry

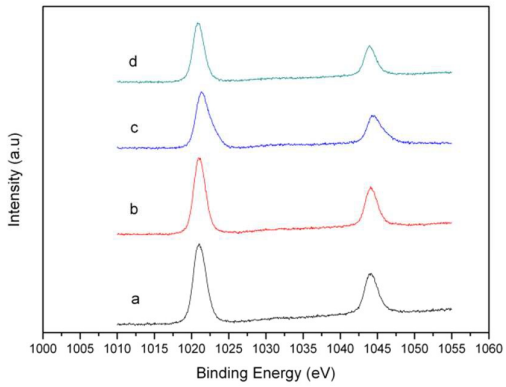

Fig.3-1. XPS analysis: Zn2p spectra of catalysts with different contents of potassium, (a) 0K-ZnCr, (b) 1K-ZnCr, (c) 3K-ZnCr and (d) 6K-ZnCr.

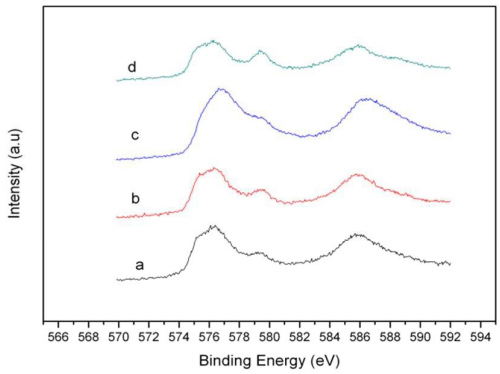

Fig.3-2. XPS analysis: Cr2p (right side) spectra of catalysts with different contents of potassium, (a) 0K-ZnCr, (b) 1K-ZnCr, (c) 3K-ZnCr and (d) 6K-ZnCr.

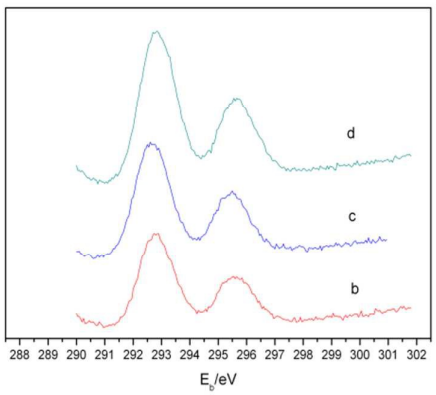

Fig.3-3. XPS analysis: K2p spectra of catalysts with different contents of potassium, (b) 1K-ZnCr, (c) 3K-ZnCr and (d) 6K-ZnCr.

Tab. 2. Bulk and surface composition of different samples

catalysts	Zn/Cr (bulk)	Zn/Cr (surface)
0K-ZnCr	0.8	0.78
1K-ZnCr	0.8	0.81
3K-ZnCr	0.8	0.79
6K-ZnCr	0.8	0.78

The powder X-ray diffractometry (XRD) patterns of Zn–Cr nanocrystals with different potassium contents are shown in Fig. 2. No diffraction peaks for potassium species were found in any of the XRD patterns. No K_2O (JCPDS card 47-1701) or K_2CO_3 (JCPDS card 49-1093) peaks were found, possibly because the K_2O phases on the spinel surfaces were highly divided. The main reflections were consistent with crystalline $ZnCr_2O_4$ (JCPDS card 22-1107), indicating that each Zn–Cr oxide sample had a spinel structure with cubic (f c c) cells. 28 No changes were found when the oxides were doped with potassium, meaning that the $ZnCr_2O_4$ phase was not affected by the addition of potassium. The particle sizes were calculated from the XRD signals using the Scherrer equation, and all of the particles were found to have diameters of around 6.0 nm regardless of the amount of potassium present. These results were consistent with the results of analyses of the TEM images of the particles. It is worth noting that no additional ZnO peaks were observed in the XRD pattern of any sample even though every sample had a Zn/Cr molar ratio greater than 0.5 (the theoretical Zn/Cr molar ratio for an ideal normal spinel). A ZnO phase may not have been detected because the ZnO phases on the spinel surfaces could have been amorphous or highly divided or because excess ZnO may have been present within the spinel structure (making the structure non-stoichiometric). In a previous study, 6 we also did not detect, using XRD, amorphous or highly divided ZnO phases on the surfaces, and we demonstrated in that study that the excess ZnO would have been present within the spinel structure (making the structure non-stoichiometric). Noritastsu 19 prepared Zn–Cr oxides with Zn/Cr molar ratios of 1 (i.e., with even higher ratios than our samples) and only found a non-stoichiometric phase, which is consistent with our results.

3.4. Characterization of the catalysts using X-ray photoelectron spectroscopy

The X-ray photoelectron spectra of the samples are shown in Figs. 3-1, 3-2 and 3-3. Features caused by the presence of Zn, Cr, and K were all found. The K 2P peaks at 292.8 eV and 295.5 eV were quite prominent. The positions of the peaks were almost the same for all of the samples, but the intensities of the peaks increased as the potassium loading increased. The spectra contained Zn 2p peaks at 1022.2 eV and 1045.2 eV and Cr^{3+} peaks at 576.4 eV and 586.0 eV, showing that the Zn and Cr species in the near-surface regions of the catalysts were primarily present as $ZnCr_2O_4$. [29] The spectrum of each catalyst also contained a Cr^{6+} peak at 578.1 eV, indicating that every catalyst had probably been over-oxidized. [30]

The Zn to Cr atomic ratios in the bulk catalysts and on the catalyst surfaces are shown in Table 2. Zinc was not found to be enriched at the surfaces of any of the catalysts. We therefore concluded that no amorphous or highly divided ZnO phases (which were also not detected using XRD) were present on the catalyst surfaces. These results indicate that the extra zinc cations were within the spinel structures, causing the spinel structures to be non-stoichiometric. [6, 31] These results are consistent with the results of our previous studies. Vaccari [31, 32] reached the same conclusions. Cations are distributed in a

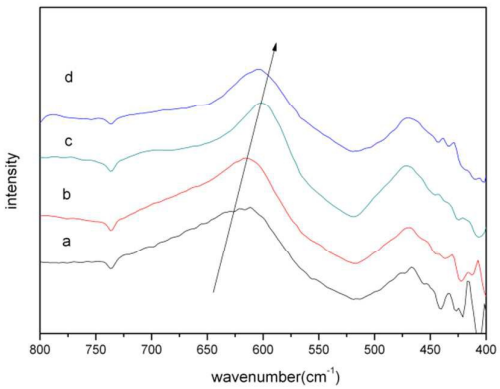

Fig. 4. The FT-IR spectra of catalysts with different contents of potassium, (a) 0K-ZnCr, (b) 1K-ZnCr, (c) 3K-ZnCr and (d) 6K-ZnCr.

more disordered fashion in non-stoichiometric spinel than in stoichiometric spinel, and, because it has more defects and oxygen vacancies that can activate reactants, non-stoichiometric spinel is a more effective catalyst than stoichiometric spinel. The non-stoichiometric spinel phase is therefore the most likely part of each of the Zn–Cr catalysts that were tested to contain the active sites involved in the formation of isobutanol. [6, 15, 31-34]

3.5 Fourier transform infrared spectral studies

The Fourier transform infrared spectra of the samples over wavenumbers 400–800 cm^{-1} are shown in Fig. 4. Two principal absorption bands, at around 475 cm^{-1} (for Cr–O vibration) and 615 cm^{-1} (for Zn–O vibration), were found. These bands were associated with $ZnCr_2O_4$, indicating that $ZnCr_2O_4$ with a spinel structure had been formed. These Cr– O and Zn–O vibration bands corresponded with the intrinsic lattice vibrations of the octahedral and tetrahedral coordination sites in the spinel structure. [35] The band at 615 cm^{-1} was blue shifted as the potassium content increased, indicating that increasing the potassium content caused more polyhedral distortion to occur. [6] Polyhedral distortion is generally closely related to disorder in the distribution of cations in a spinel structure. A more disorderly cation distribution will cause more polyhedral distortion to occur in a $ZnCr_2O_4$ spinel structure. The blue shift of the 615 cm^{-1} band therefore showed that increasing the potassium content caused the cation distribution to become more disordered.

3.6. Rietveld analysis of the catalysts

A spinel structure contains two types of cation site, tetrahedral and octahedral sites. In an ideal normal Zn–Cr spinel, Zn cations occupy the tetrahedral sites and Cr cations occupy the octahedral sites. In contrast, in an ideal inverse spinel, Zn cations occupy the octahedral sites and half of the Cr cations occupy the tetrahedral sites. However, most spinel compounds deviate from the ideal normal/inverse spinel distributions. The species occupying the two types of site are affected by various factors, such as the calcination temperature, cation charges, electronic states, ion sizes, and particle sizes. The physical and chemical properties of a material with a spinel structure can be tailored by controlling the cations that occupy the tetrahedral and octahedral coordination sites. It was therefore crucial for us to investigate the cation distributions in the Zn–Cr spinel structures in our catalysts.

The Rietveld method can be used to determine the characteristics of a single crystal structure, including the atom positions, fractional occupancies, lattice parameters, and thermal parameters. [36-41] Information on the structures and microstructures of all of our materials was acquired by analyzing the XRD patterns of the materials using the Rietveld program "FP_Suite_TB". Crystal refinements were performed assuming that the materials each had a cubic crystallographic structure with the space group Fd-3m. A few parameters, including the background parameters, cell parameter 'a', scale factor, site occupancy parameters, and zero point for 2θ, were fitted to the data points for each material.

The profile fitting qualities for the 0K-ZnCr sample are shown in Fig. 5-1. The profiles for the others samples were similar, as shown in Fig. 5-2. An approximately straight line was found for the differences between the calculated and observed patterns, implying that the simulated results were reliable. The cell-parameter data results for the $ZnCr_2O_4$ spinel (spinel-like) phase are shown in Table 3. The lattice parameters for all of the samples were larger than the lattice parameters for the JCPDS standard (a=b=c=8.3275 Å), and the parameters increased as the potassium content increased. The lattice parameters for a spinel structure will generally vary depending on the average radii of the cations in the tetrahedral and octahedral sites. This means that the entire spinel framework will grow or contract to accommodate cations of different sizes when the metals in the tetrahedral and octahedral sites are changed. [42] The differences between the lattice parameters for our samples would therefore have been caused by the samples having different degrees of disorder in the cation distributions.

The estimated cation distribution data for the $ZnCr_2O_4$ spinel phase, found through Rietveld analysis, are shown in Table 4. Variations in the cation distributions in the $ZnCr_2O_4$ spinel structures can clearly be seen in Table 4. The percentage of Zn^{2+} cations that were disordered (in octahedral vacancies)

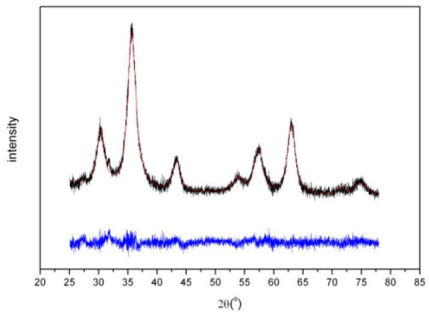

Fig.5-1. XRD patterns of 0K-ZnCr. The black curve is the experimental points, the red curve is the pattern calculated by Rietveld analysis. The difference (the blue curve) between the calculated and observed pattern is presented below the corresponding diffractogram.

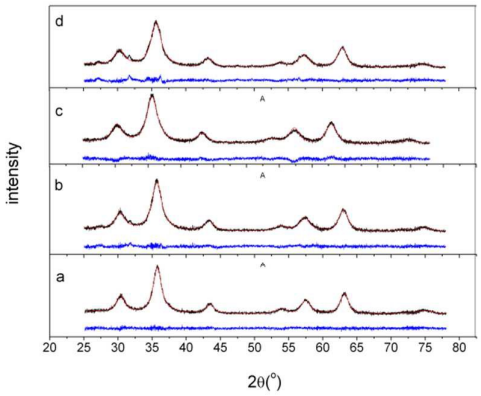

Fig.5-2. XRD patterns with different contents of potassium, (a) 0K-ZnCr, (b) 1K-ZnCr, (c) 3K-ZnCr and (d) 6K-ZnCr. The black curve is the experimental points, the red curve is the pattern calculated by Rietveld analysis. The difference (the blue curve) between the calculated and observed pattern is presented below the corresponding diffractogram.

Tab. 3. Cell-parameter data of $ZnCr_2O_4$ spinel (spinel-like) phase estimated from the Rietveld analysis

catalysts	Cell-parameters (a=b=c)/Å
0K-ZnCr	8.3376
1K-ZnCr	8.3464
3K-ZnCr	8.3597
6K-ZnCr	8.3599

Tab. 4. Cation distribution data of $ZnCr_2O_4$ spinel (spinel-like) phase estimated from the Rietveld analysis

Cations	Occupied percentage			
	0K-ZnCr	1K-ZnCr	3K-ZnCr	6K-ZnCr
Zn_1	0.8518	0.8245	0.8097	0.7957
Cr_1	0.1469	0.1730	0.1929	0.1987
Zn_2	0.1379	0.1787	0.2154	0.2201
Cr_1	0.8467	0.8075	0.7957	0.7798

Zn_1 (Cr_1) represents Zn^{2+} (Cr^{3+}) in tetrahedral vacancies while Zn_2 (Cr_2) represents Zn^{2+} (Cr^{3+}) in octahedral vacancies.

increased linearly from 13.79% to 21.54% as the potassium content increased from 0% to 3% and then increased slightly to 22.01% when the potassium content increased to 6%. The percentage of Cr^{3+} cations that were disordered (in tetrahedral vacancies) followed a similar trend to the percentage of Zn^{2+} cations that were disordered. To simplify our discussion, therefore, we will only consider the distribution of Zn^{2+} in the spinel structure below.

We may cautiously conclude from Tables 3 and 4 that every sample had a different degree of cation disorder and that increasing the potassium content increased the degree of cation disorder. The metal cations in samples with large particles and normal spinel structures will generally be in the thermodynamically most stable sites of the bulk material. However, our samples had quite small particles (about 6 nm in diameter), meaning that a large fraction of the metals in each particle would have been at the surface. Surface truncation would have led to there being large numbers of dangling bonds, which would affect the bonding environments of the metals. Our characterization results and Rietveld calculation results indicated that the lowest-energy configurations of the metals were satisfied by the distributions of disordered cations. We could therefore postulate that the potassium present could affect the cation distribution by affecting the bonding environment. This will be discussed further below. Nordhei [43] also stated that the coordination of surface metal ions will be distorted by adsorbed oxygen and water or because of the presence of hydroxides, and that would affect the distribution of disordered cations.

3.7. Analysis of the catalysts using oxygen X-ray photoelectron spectroscopy

The O 1s X-ray photoelectron spectra of the catalysts with different potassium contents are shown in Fig. 6. All of the samples had three predominant peaks, at ~529.4 eV, 531.1 eV, and 532.7 eV, which were attributed to lattice oxygen (O_{latt}), surface-adsorbed oxygen (O_{ads}), and surface hydroxyl species (O_{OH-}), respectively. [44] The (O_{OH-} + O_{ads}) / (O_{latt} + O_{OH-} + O_{ads}) molar ratio for each sample was determined by quantitatively calculating the appropriate peak areas, and the ratios are shown in Table 5. The (O_{OH-} + O_{ads}) / (O_{latt} + O_{OH-} + O_{ads}) ratio increased as the potassium content increased from 0% to 3% and then decreased slightly as the potassium content increased to 6%. This was confirmed by performing a H_2 temperature-programmed reduction (TPR) study on each sample, the results of which are shown in Fig. 7. As mentioned above, a spinel with disordered cations will be in a metastable state, which could be stable because of the presence of a large number of dangling bonds (O_{ads} and O_{OH-}). The number of dangling bonds will increase as the potassium content increases, causing more cations to be disordered as the potassium content increases, which is consistent with our Rietveld calculations. The (O_{OH-} + O_{ads}) / (O_{latt} + O_{OH-} + O_{ads}) ratio was slightly lower for the sample with a potassium content of 6% than for the sample with a potassium content of 3%, possibly because the S_{BET} decreased when the potassium content was increased from 3% to 6% (as shown in Table 1). More interestingly, the position of the O_{OH-} peak shifted to a higher binding energy as the potassium content increased. This would have caused the difference between the binding energies of the O_{OH-} and Zn 2p core levels to decrease significantly as the potassium content increased, indicating that the stabilities of the O_{OH-} were enhanced by the presence of potassium. [45] The results of the CO-infrared analysis described below suggested that the O_{OH-} not only play crucial roles in stabilizing the metastable state but also facilitate the synthesis of alcohols. Producing more stable O_{OH-} will therefore be another non-ignorable factor when attempting to improve the activities of catalysts for the synthesis of isobutanol.

3.8. H_2-TPR analysis of the catalysts

The redox properties of the different catalysts were evaluated by performing H_2-TPR analyses of the catalysts, and the results are shown in Fig. 7. Each catalyst had only one main hydrogen consumption peak in the temperature range 300–400 °C. The area of this peak increased as the potassium content increased from 0% to 3% and then decreased slightly as the potassium content increased to 6%. An accurate evaluation of the redox properties of the catalysts required quantitative analyses to be performed. The hydrogen consumption values for the 0K-ZnCr,

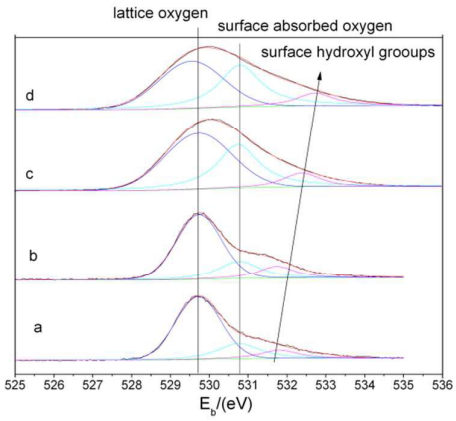

Fig. 6. O 1s XPS spectra of catalysts with different contents of potassium, (a) 0K-ZnCr, (b) 1K-ZnCr, (c) 3K-ZnCr and (d) 6K-ZnCr.

Tab.5. O species surface composition of different catalysts

Catalysts	Oads/(Olatt + Oads + O_{OH-})	O_{OH-}/(Olatt + Oads + O_{OH-})
0K-ZnCr	0.13	0.09
1K-ZnCr	0.16	0.11
3K-ZnCr	0.21	0.13
6K-ZnCr	0.20	0.13

1K-ZnCr, 3K-ZnCr and 6K-ZnCr samples were about 0.61 mmol/g, 0.97 mmol/g, 1.24 mmol/g, and 1.01 mmol/g, respectively. It has previously been found that Zn^{2+} and Cr^{3+} in Zn–Cr spinel are very difficult to reduce. However, each of our catalysts was in a "metastable state" because of the presence of disordered cations, and this would have allowed our catalysts to be reduced much more easily than Zn–Cr spinel. Our previous X-ray absorption spectroscopy analyses of the samples showed that the Zn and Cr absorption edges were at higher energies in our samples than in Zn–Cr spinel, meaning that the Zn and Cr valences were higher in our samples than in normal spinel. This meant that our catalysts could be reduced much more easily than normal spinel. We attributed the increasing hydrogen consumption as the potassium content increased from 0% to 3% to the number of oxygen-containing species on the surfaces of the particles increasing as the potassium content increased. The area of the reduction peak decreased slightly when the potassium content was increased from 3% to 6%, and we attributed this to the number of oxygen-containing species decreasing (as shown in Table 5). These results are consistent with the oxygen X-ray photoelectron spectroscopy (XPS) results.

Potassium is a good electron promoter, and can transfer charge to the active phase and increase the charge density. This means that the presence of potassium will change the reducibility of a Zn–Cr catalyst and therefore change the ability of the catalyst to catalyze the synthesis of isobutanol. This could be why the presence of potassium could change the

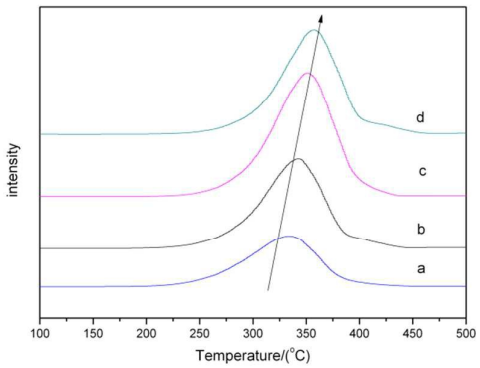

Fig.7. H_2-TPR profiles of catalysts, (a) 0K-ZnCr, (b) 1K-ZnCr, (c) 3K-ZnCr and (d) 6K-ZnCr.

number of dangling bonds present (shown in Fig. 6). The reduction peak was shifted to a higher temperature as the potassium content increased, showing that the oxygen-containing species on the catalyst surfaces became more stable as the potassium content increased (consistent with our oxygen XPS analysis results). Tsubaki et al. [19] also suggested that alkali metals can change the redox properties of catalysts and dramatically affect the distributions of the alcohols produced using the catalysts. They confirmed that alkali metals are good electronic assistants in the transfer of charge to the active phase of non-stoichiometric spinel $Zn_xCr_{2/3(1-x)}O$, increasing the charge density and improving the catalytic performance.

3.9. CO-IR analysis of the catalysts

Additional information on the identities and populations of the species present after CO molecules had been adsorbed at the reaction temperature was acquired by performing an in situ Diffuse Reflectance Infrared Fourier Transform Spectroscopy (DRIFTS) study. The consumption of hydroxyl species (determined by measuring the peak at 3400 cm^{-1}) when each catalyst with adsorbed CO molecules had been reacted is shown in Fig. 8 (on the left). The amount of hydroxyl consumed increased as the potassium content increased, showing that the amount of hydroxyl on the catalyst surface increased as the potassium content increased. This result agreed with the XPS and H_2-TPR analysis results. The C_1 species produced after the adsorbed CO had reacted with the surface hydroxyl species are shown for each catalyst in Fig. 8 (on the right). Two main C_1 species were found, formate species (determined from peaks at 1600 cm^{-1}, $\upsilon_{as}(CO^{2-})$ and 1375 cm^{-1}, σ(CH)) and carbonate species (determined from peaks at 1510 cm^{-1} and 1330 cm^{-1}). [46, 47] The spectrum for catalyst 0K-ZnCr showed that mostly carbonates had formed, the formate signal being only small. The formate species population increased as the potassium content increased, reaching a maximum at a potassium content of 3%. The carbonate species population followed the opposite trend.

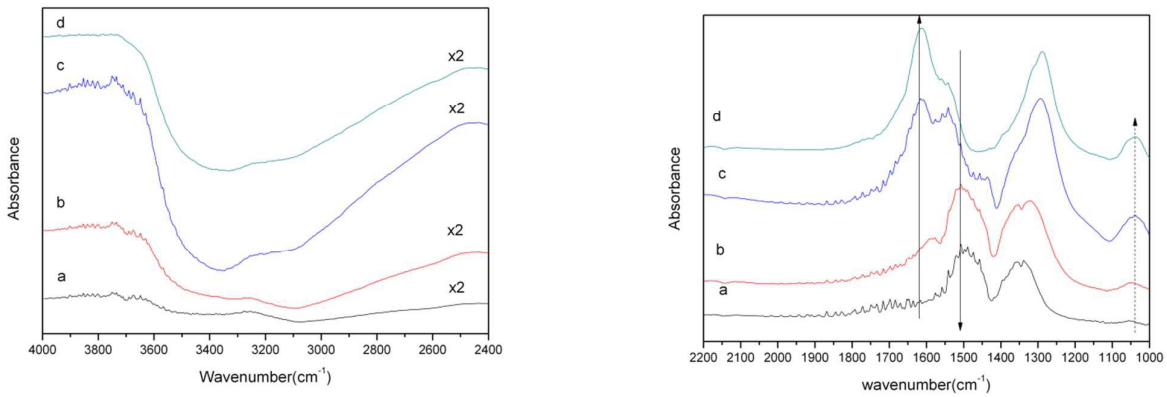

Fig. 8. DRIFTS spectra of CO adsorbed on catalysts upon desorption at 400 °C, left side: the consumption of hydroxyl species after reaction with adsorbed CO molecule, right side: corresponding C1 species after adsorbed CO reaction with surface hydroxyl species, (a) 0K-ZnCr, (b) 1K-ZnCr, (c) 3K-ZnCr and (d) 6K-ZnCr.

Bell and co-workers [46] suggested that the formate species forms through an activated process, most probably involving the transfer of a proton from a surface hydroxyl group to adsorbed CO, and that carbonate species form through interactions between CO and both O^{2-} and OH^- sites on ZrO_2 surfaces. Using a temperature programmed surface reaction, Wachs and Madix [46] discovered that formate is a stable intermediate in the reaction of CO/CO_2 to give CH_3OH whereas carbonate species can easily be converted to CO_2, which is not able to be used to synthesize alcohols. Waugh [48] concluded that formate is a true intermediate and is the most stable and long-lived intermediate in the synthesis of methanol. Some conclusions could cautiously be drawn from the discussion above. The formate species is a very significant intermediate in the synthesis of methanol, and the formation of formate involves hydroxyl groups and adsorbed CO on the catalyst surfaces. For our catalysts, taking into consideration the results of the in situ DRIFT analyses (shown in Fig. 8) and the performances of the catalysts (shown in Table 6), it seems that the surface hydroxyl species not only stabilized the metastable state but also facilitated the formation of formate, which is a very significant intermediate C_1 species in the synthesis of alcohols.

3.10. Catalytic activity measurements

The catalytic activities of the samples for the synthesis of isobutanol and MeOH are shown in Table 6. Only ~10% of the CO was converted by the 0K-ZnCr catalyst, and the selectivity for isobutanol was poor (isobutanol contributed 9.09% of the alcohols produced). Adding the potassium promoter increased the amount of CO that was converted, ~17% and ~26% of the CO being converted by the 1K-ZnCr and 3K-ZnCr samples, respectively, and improved the selectivity for isobutanol to 18.55% (for the 3K-ZnCr sample). However, increasing the potassium content to 6% caused the CO conversion rate to decrease to ~18% and the selectivity for isobutanol to decrease to 11.04%.

The Zn–Cr catalysts that we tested were less selective for isobutanol than were the Zn–Cr catalysts tested by Epling and co-workers,[11,12] possibly because different reaction conditions and/or sample compositions and textures were used. It must be stressed that our study was not aimed at improving the selectivity for isobutanol but to investigate the role of the potassium promoter in the formation of isobutanol on Zn–Cr spinel catalysts.

The catalysts containing the potassium promoter had much higher activities and much better selectivities for isobutanol than did the catalyst containing no potassium. Increasing the potassium content from 0% to 3% doubled the CO conversion rate (from 12.96% to 26.09%) and the isobutanol selectivity (from 9.09% to 18.55%). The activity and isobutanol selectivity would have increased because of the positive influence exerted by the potassium promoter. The CO conversion rate and isobutanol selectivity would have been poorer for the 6K-ZnCr catalyst than for the 3K-ZnCr catalyst because the 6K-ZnCr catalyst contained an excess of potassium. The excess potassium would have been unevenly distributed, and would have partly covered the active sites at which isobutanol could have been formed, negatively affecting the catalyst performance. The optimum potassium content in our samples was therefore 3%. It is worth noting that the selectivity for methanol plus isobutanol was close to 95% (i.e., methanol and isobutanol contributed 95% of the alcohols produced), which is typical for Zn–Cr catalysts. Using catalysts such as those we tested should allow the separation of the products of isobutanol production reactions to be simplified, making the industrial-scale production and use of isobutanol possible.

In our analyses we found some interesting phenomena that could explain the positive influence of the potassium promoter. As may have been noticed, the cation distribution and the states of the oxygen species on the Zn–Cr spinel surfaces could be affected by the potassium promoter. In our previous work [6] we found that the productivity of a system and the selectivity for isobutanol are strongly related to the cation distribution in the Zn–Cr spinel catalyst used. More disorder in the cation

Tab. 6. Typical catalytic performance of Zn-Cr based catalysts

catalysts	CO conversion (%)	Alcohol selectivity (%)	Total alcohol rate (g/ml h)	Alcohol distribution /wt%				
				Methanol	Ethanol	Propanol	Isobutanol	C_{5+} alcohol
0K-ZnCr	12.96	40.84	0.066	87.67	0.92	0.43	9.09	0.27
1K-ZnCr	17.96	42.84	0.079	79.01	0.81	1.93	15.82	0.92
3K-ZnCr	26.09	46.71	0.093	76.58	2.51	1.33	18.55	1.03
6K-ZnCr	18.16	45.51	0.086	78.53	2.58	6.33	11.04	1.03

Reaction conditions: Temperature=400^{o}C, Pressure=10 Mpa, GHSV=3000 h^{-1}

distribution means that the crystal will be less perfect, there will be more oxygen vacancies, and there will be more defects, meaning that the activation energy for the production of However, the rather small particles (about 6 nm in diameter) in our catalysts meant that a large proportion of the metal ions would have been at the surface, meaning that the catalysts would have had some disordered cations. The distribution of the disordered cations would not have been stable. Large numbers of dangling bonds (O_{ads} and O_{OH-}) would have been needed to stabilize the metastable state. We found that the potassium promoter could stabilize the metastable state by increasing the populations and stabilities of the dangling bonds (O_{ads} and O_{OH-}). More importantly, we found that these dangling bonds could not only play a crucial role in stabilizing the metastable state but also facilitate the formation of formate, which is a very significant intermediate C_1 species in the synthesis of alcohols. This knowledge is likely to be extremely useful for improving the performances of catalysts for the formation of isobutanol. In conclusion, the presence of potassium causes the cations to be disordered, which dramatically affects the states of the oxygen species on the catalyst surfaces and makes the formation of isobutanol more effective.

4. Conclusion

A series of Zn–Cr oxide nanoparticles with different potassium contents were produced using a coprecipitation and post-calcination method. The phases and particle sizes of the catalysts were determined using TEM and XRD. Fourier transform infrared spectroscopy, XPS, and Rietveld analyses were used to determine the different distributions of disordered cations in the different Zn–Cr spinel samples. We showed that the potassium promoter strongly affected the cation distribution in the Zn–Cr spinel and that the effects increased as the potassium content increased. The strongest effects were found for the 3K-ZnCr catalyst. The CO conversion of 3K-ZnCr catalyst reaches to the highest (~26%) and the alcohol selective and isobutanol selective will also are the best among all of catalysts, which reach to 46.71% and 18.55%, respectively.

The potassium promoter was also found to strongly affect the states of the oxygen species on the surfaces of the Zn–Cr spinel. Both the populations and the stabilities of the oxygen species were found to be enhanced by the presence of potassium. In situ DRIFT analysis and the catalytic isobutanol will be lower. To be specific, the metals in bulk spinel will be in the thermodynamically most stable sites, giving a normal spinel structure (without disordered cation performances showed that surface hydroxyl species not only stabilized the metastable state but also facilitated the formation of formate, which is a very significant intermediate C_1 species in the synthesis of alcohols.

The activity and selectivity of a catalyst were found to be closely related to the potassium content of the catalyst. The optimum potassium content for our samples was found to be 3%. Higher or lower potassium contents gave poorer catalytic performances. This clearly demonstrates that adding a potassium promoter will be one of the crucial factors in improving the performances of Zn–Cr catalysts for the synthesis of isobutanol. Using a catalyst with an optimum potassium content will cause the optimum number of disordered cations to be present. The effect of this on the states of the oxygen species on the surfaces of the catalyst will allow isobutanol to be formed more effectively than when a catalyst using a non-optimum potassium content is used.

Acknowledgements

This work was supported by the National Natural Science Foundation of China (21573269), the Prospective Project of Institute of Coal Chemistry, The Chinese Academy of Sciences (No. 2011SQZBJ13) and the Cooperative Project of Shaanxi Yanchang Petroleum (Group) Corp. Ltd., China (JT1014SKF0003).

Notes and references

1. Y. Wu, H. Xie, S. Tian, N. Tsubaki, Y. Han and Y. Tan, *J. Mol. Catal. A: Chem.* , 2015, 396, 254-260.
2. M. Xu, M. J. L. Gines, A. M. Hilmen, B. L. Stephens and E. Iglesia, *J. Catal.* , 1997, 171, 130-147.
3. D.V. N. Vo and A. A. Adesina, *Catal. Sci. Technol.*, 2012, 2, 2066-2076.
4. M. M. Lv, W. Xie, S. Sun, G. M. Wu, L. R. Zheng, S. Q. Chu, C. Gao and J. Bao, *Catal. Sci. Technol.*, 2015, 5, 2925-2934.
5. M. T. Claure, S. H. Chai, S. Dai, K. A. Unocic, F. M. Alamgir, P. K. Agrawal and C. W. Jones, *J. Catal.* , 2015, 324, 88-97.
6. S. Tian, S. Wang, Y. Wu, J. Gao, Y. Bai, P. Wang, H. Xie, Y. Han and Y. Tan, *J. Mol. Catal. A: Chem.* , 2015, 404–405, 139-147.
7. P. Forzatti, E. Tronconi and I. Pasquon, *Catal. Rev.*, 1991, 33, 109-168.

8. Y. P. Xu, P. G. Duan and F. Wang, *Fuel Process. Technol.* , 2015, 130, 268-274.
9. Z. F. Chang, P. G. Duan and Y. P. Xu, *Bioresour. Technol.* , 2015, 184, 349-354.
10. L. Lietti, E. Tronconi and P. Forzatti, *J. Catal.* , 1992, 135, 400-419.
11. W. S. Epling, Gar B. Hoflund, Walter M. Hart and Y. D. M. Minahan, *J. Catal.*, 1997, 169, 438-446.
12. W. S. Epling, Gar B. Hoflund, W. M.Hart and Y. D. M. Minahan, *J. Catal.*, 1997, 172, 13-23.
13. R. G. Herman, *Catal. Today* 2000, 55, 233-245.
14. W. Keim and W. Falter, *Catal. Lett.* , 1989, 3, 59-63.
15. G. D. Piero, F. Trifiro and A. Vaccari, *J. Chem. Soc., Chem. Comm.*, 1984, 656-658.
16. S. Tian, S. Wang, Y. Wu, J. Gao, H. Xie, X. Li, G. Yang, Y. Han and Y. Tan, RSC Advances, 2015, 5, 89273-89281.
17. Y. Q. Wu, H. J. Xie, Y. L. Kou, N. Tsubaki, Y. Z. Han and Y. S. Tan, Korean J. Chem. Eng. , 2015, 32, 406-412.
18. Y. Kou, H. Xie, G. Liu, Y. Wu, X. Zhang, Y. Han, T. Noritatsu and Y. Tan, J. Fuel Chem. Technol., 2013, 41, 703-709.
19. L. Tan, G. Yang, Y. Yoneyama, Y. Kou, Y. Tan, T. Vitidsant and N. Tsubaki, *Appl. Catal., A-gen* , 2015, 505, 141-149.
20. J. S. Lee, S. Kim and Y. G. Kim, *Top. Catal.* , 1995, 2, 127-140.
21. J. Iranmahboob, D. O. Hill and H. Toghiani, *Appl. Surf. Sci.* , 2001, 185, 72-78.
22. W. Sachtler, D. Shriver, W. Hollenberg and A. Lang, *J. Catal.* , 1985, 92, 429-431.
23. S. Zaman and K. J. Smith, *Catal. Rev.*, 2012, 54, 41-132.
24. N. Koizumi, K. Murai, T. Ozaki and M. Yamada, *Catal. Today* 2004, 89, 465-478.
25. Z. Y. Liu, X. G. Li, M. R. Close, E. L. Kugler, J. L. Petersen and D. B. Dadyburjor, *Indu. & Engi. Chem. Res.* 1997, 36, 3085-3093.
26. M. L. Xiang, D. B. Li, J. Zou, W. H. Li, Y. H. Sun and X. C. She, *J. Nat. Gas Chem.* , 2010, 19, 151-155.
27. A. Riva, F. Trifirò, A. Vaccari, L. Mintchev, D. Sanfilippo and W. Manzatti, *J. Chem. Soc., Fara. Trans.*, 1987, 83, 2213-2225.
28. S. Chen, Y. Wu, P. Cui, W. Chu, X. Chen and Z. Wu, *The J. Phys. Chem. C*, 2013, 117, 25019-25025.
29. A. Venugopal, R. Sarkari, C. Anjaneyulu, V. Krishna, M. K. Kumar, N. Narender and A. H. Padmasri, *Appl. Catal., A-gen* , 2014, 469, 398-409.
30. S. A. Hosseini, M. C. Alvarez-Galvan, J. L. G. Fierro, A. Niaei and D. Salari, *Ceram. Int.* , 2013, 39, 9253-9261.
31. E. Giamello, B. Fubini, M. Bertoldi, G. Busca and A. Vaccari, J. Chem. Soc., Fara. Trans., 1989, 85, 237.
32. E. Errani, F. Trifiro, A. Vaccari, M. Richter and G. Delpiero, *Catal. Lett.* , 1989, 3, 65-72.
33. M. Bertoldi, B. Fubini, E. Giamello, G. Busca, F. Trifirò and A. Vaccari, *J. Chem. Soc., Fara. Trans.*, 1988, 84, 1405.
34. b. F. T. Gastone Del Piero, Angelo Vaccari, *J. Chem. Soc., Chem. Commun.*, 1984, 656-658.
35. S. A. Gene, E. Saion, A. H. Shaari, M. A. Kamarudin, N. M. Al-Hada and A. Kharazmi, *J. Nanomater.*, 2014, 7.
36. P. A. Deshpande, S. T. Aruna and G. Madras, *Catal. Sci. Technol.*, 2011, 1, 1683-1691.
37. R. A. Roca, J. C. Sczancoski, I. C. Nogueira, M. T. Fabbro, H. C. Alves, L. Gracia, L. P. S. Santos, C. P. de Sousa, J. Andres, G. E. Luz, E. Longo and L. S. Cavalcante, *Catal. Sci. Technol.*, 2015.
38. C.-C. Hu, T.-F. Yeh and H. Teng, *Catal. Sci. Technol.*, 2013, 3, 1798-1804.
39. T. V. B. Pantelis N. Trikalitis, Aliki C. Moukarika, Antonios Sdoukos Thomas Angelidis, Philip J. Pomonis, *Appl. Catal., A-gen.*, 1998, 167, 295-308.
40. J. F. Brazdil, *Catal. Sci. Technol.*, 2015, 5, 3452-3458.
41. R. Poreddy, C. Engelbrekt and A. Riisager, *Catal. Sci. Technol.*, 2015, 5, 2467-2477.
42. C. Wang, S. Yang, H. Chang, Y. Peng and J. Li, *J. Mol. Catal. A: Chem.* , 2013, 376, 13-21.
43. C. Nordhei, A. L. Ramstad and D. G. Nicholson, *PCCP* 2008, 10, 1053-1066.
44. C. H. Zhang, C. Wang, W. C. Zhan, Y. L. Guo, Y. Guo, G. Z. Lu, A. Baylet and A. Giroir-Fendler, *Appl. Catal. B-Environ.*, 2013, 129, 509-516.
45. B. Mallesham, P. Sudarsanam, G. Raju and B. M. Reddy, *Green Chem.* , 2013, 15, 478-489.
46. K. Pokrovski, K. T. Jung and A. T. Bell, *Langmuir*, 2001, 17, 4297-4303.
47. A. Riva, F. Trifirò, A. Vaccari, L. Mintchev and G. Busca, *J. Chem. Soc., Fara. Trans.*, 1988, 84, 1423.
48. K. C. Waugh, *Catal. Lett.* , 2012, 142, 1153-1166.

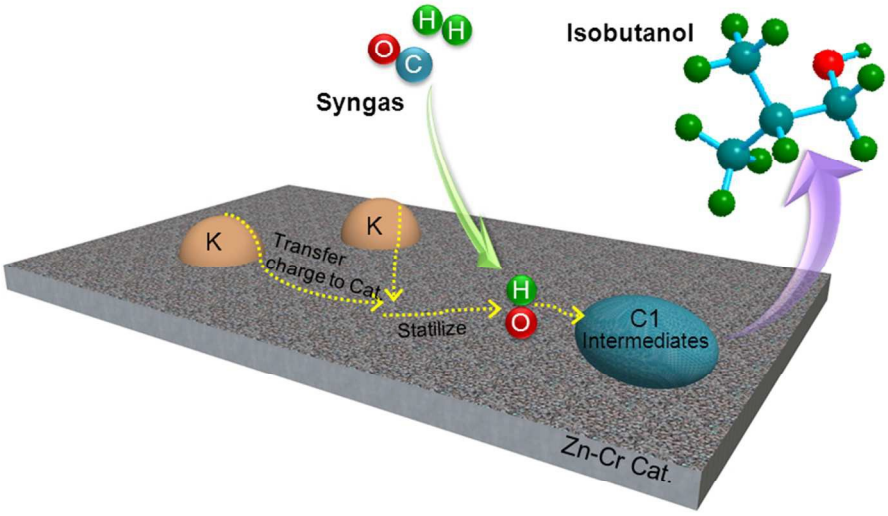

254x190mm (96 x 96 DPI)